Heliyon 8 (2022) e12396

Contents lists available at ScienceDirect

Heliyon

journal homepage: www.cell.com/heliyon

Research article

Affinity of carbon quantum dots anchored within metal organic framework matrix as enhancer of plant nourishment

Hanan B. Ahmed [a,**], Noura E. Mahmoud [b], Asmaa A. Mahdi [b], Hossam E. Emam [c,*], Reda M. Abdelhameed [d,***]

[a] Chemistry Department, Faculty of Science, Helwan University, Ain-Helwan, Cairo 11795, Egypt
[b] Biochemistry Unit, Plant Genetic Resources Department, Desert Research Center, Cairo, Egypt
[c] Department of Pretreatment and Finishing of Cellulosic based Textiles, Textile Research and Technology Institute, National Research Centre, 33 EL Buhouth St., Dokki, Giza 12622, Egypt
[d] Applied Organic Chemistry Department, Chemical Industries Research Institute, National Research Centre, 33 EL Buhouth St., Dokki, Giza 12622, Egypt

GRAPHICAL ABSTRACT

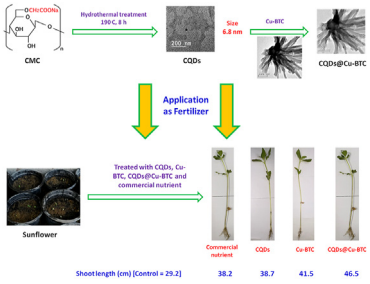

ARTICLE INFO

Keywords:
Carbon quantum dots
Metal organic framework
Sunflower
Fertilizer
Photosynthetic pigments

ABSTRACT

Nano-fertilizers were ascribed to be significantly advantageous with minimizing the negative effects of requiring excessive contents in the soil and reducing the number of times for fertilization. Herein, the superior affinity of carbon quantum dots (CQDs) anchored within metal organic framework (Cu-BTC) matrix was investigated for the first time as a fertilizer for sunflower. CQDs were nucleated from alkali-hydrolyzed carboxymethyl cellulose (CMC) via the hydrothermal technique. The synthesized CQDs (6.8 ± 3.7 nm) were anchored within Cu-BTC (crystalline rod-like structure) matrix, to produce CQDs@Cu-BTC composite. The obtained CQDs and CQDs@Cu-BTC were applied as nutrients for the sunflower plant. The chlorophyll a and carotenoids contents were 0.465 & 0.497 and 0.350 & 0.364 mg/g after treatment with CQDs & CQDs@Cu-BTC, respectively. The shoot length of sunflower sample was increased after feeding with CQDs and CQDs@Cu-BTC to be 38.7 and 46.5 cm, respectively. The obtained results confirmed that, the synthesized CQDs@Cu-BTC showed superiority as nutrient material via enhancing the growth and physiological properties of sunflower and consequently could be used as fertilizer for plants instead of the commercial nutrient.

* Corresponding author.
** Corresponding author.
*** Corresponding author.
E-mail addresses: hananbasiony@gmail.com (H.B. Ahmed), hossamelemam@yahoo.com (H.E. Emam), reda_nrc@yahoo.com (R.M. Abdelhameed).

https://doi.org/10.1016/j.heliyon.2022.e12396
Received 23 July 2022; Received in revised form 2 October 2022; Accepted 8 December 2022

1. Introduction

The nano-formulated elements could hold a great promise for their application in different purposes including catalysis and plant nourishment, attributing to their unique optical properties, size-dependent qualities and high surface area [1, 2, 3, 4, 5, 6]. Whereas, their high surface area increases the amounts of the atoms on the surface, that could serve as a bio-protective source and as a beneficial food source [7, 8]. Nano-fertilizers were reported to promote the efficiency of the crop nutrient and rate of growth through the reduction of the soil toxicity, minimizing the negative effects of the excessive contents of the fertilizer in the soil and reduce the number of times for applying the fertilizer [9, 10]. Via the utilization of the nano-fertilizers, the time of releasing and speed of the elements could be in line with the nutritional requirements of the plant. Accordingly, the plant can absorb the highest amounts of nutrients and in turn reducing the leaching out of the elements and increases the cropping yield [11, 12, 13, 14].

Carbon quantum dots (CQDs) as superiorly investigated carbon-based nano-materials, have extensively attracted the attention owing to their excellent characters like its outstanding optical activities, high photo-stabilities, and low toxic effects. CQDs were potentially applicable in different purposes such as sensing, photo-catalysis, solar cells, bio-imaging, drug delivery and photovoltaic tools [15, 16, 17, 18, 19, 20, 21, 22, 23]. Most of CQDs that were synthesized in various approaches were shown to exhibit hydrophilic characters and always were interestingly considered with the researchers. Qu et al. were studied the synthesis of water-soluble/photoluminescent carbon quantum dots by microwave-assisted technique, that could be exploited as bio-compatible/optically active ink for various purposes [24]. Di et al. reported that carbon nanodots could be synthesized with high affinity for water solubilization and that could be applied for sensitive estimation of arsenite [25].

After Qu et al. [24] were revealed the biocompatibility of CQDs with bean sprouts, the potentiality of CQDs on the growth of the crops was world widely attracted the attention of researchers. The superior potency of CQDs in the physiological processing of plants was demonstrated, including the growth, photosynthesis, and resistance to the biotic/abiotic stress [26, 27, 28]. Moreover, treatment of plants with CQDs was also shown its enhanced impacts on the fixation of biological nitrogen by azotobacter [29]. Additionally, CQDs were played the role of delivering siRNA in the model plants [29, 30].

MOFs could be successfully applied as fertilizers, as they contain the essential elements required as nutrients for the crops, such as nitrogen, phosphorus, and the metal micro-nutrients, such as iron, zinc, etc. Various reports were considered with the effects of different types of MOFs on the growth rate of different plants while, they were verified the potentiality of MOF as fertilizers. Oxalate-phosphate-amine metal-organic-frameworks (OPA-MOFs) were studied for its effects on the growth, nutrient uptake and grain yield of wheat, whereas, the results showed that OPA-MOF exhibited a high potentiality for enhancement the efficiency of nitrogen fertilizer [31, 32].

Moreover, iron-metal-organic-frameworks-ethylene diamine tetra-acetic acid (Fe-MOF-EDTA) was exploited as iron sources in Phaseolus vulgaris, whereas, by comparing with the other iron sources, the Fe-MOF-EDTA showed to improve the chlorophyll content, protein and enzymes activities and enhancement percent of 9.6% in the plant weight [33]. Another study also showed that oxalate could increase the phosphorous bio-availability in the soil [34]. Whereas, oxalotrophic bacteria that could mostly exist in all types of soils for phosphorous bio-availability, use the oxalate as a carbon source as it could satisfy their requirements for energy in the metabolism, leading to produce carbonates, as this metabolic process is known as oxalate-carbonate pathway [35, 36]. From this point, MOFs that are based on oxalate as organic ligand could be successfully exploited as plant fertilizers.

Copper-based metal organic frameworks were also abbreviated as MOF-199, HKUST-1 and Cu-BTC with common name of basolite were widely applicable in wastewater treatment for the removal of heavy metals and other toxic contaminants [37]. Cu-MOF was reported to exhibit an octahedral structural shape. Cu-MOF is advantageous with high potentiality for gas storage and capturing, attributing to its porosity, high surface area and simplicity for its synthesis [38]. There were several reported methodologies for synthesis of Cu-MOF that were conventionally known such like, mechanochemical, hydrothermal, sonochemical, and microwave-assisted techniques [39]. However, the relative crystallinity and morphological features of the synthesized MOF were variably dependent on the applied synthetic methodology. The hydrothermal methodology is known as the standard method for synthesis of MOF, but disadvantageous with long duration from several hours to days. The mechanochemical technique is characteristic as solvent less procedure. In sonochemical methodology, the ultrasonic wave is used for fast heating and cooling. However, microwave-assisted technique promotes manipulate power output for heating at specific time. All of the as-mentioned methodology involved the interaction of copper salt with 1, 3, 5-benzene tricarboxylic acid (BTC) or 1, 4-benzene dicarboxylic acid (H2BDC) as organic ligand.

Accordingly, the point of novelty in the current approach is the investigation of the affinity for CQDs@Cu-BTC composite as a fertilizer for contribution in improving the morphological and physiological properties of sunflower. In the current approach, CQDs were nucleated from alkali-hydrolyzed carboxymethyl cellulose (CMC) via the hydrothermal technique. Afterword, the synthesized CQDs was anchored within Cu-BTC (MOF) matrix, in order to produce CQDs@Cu-BTC composite. The synthesized CQDs were characterized via FTIR, NMR & TEM analyses. Additionally, Cu-BTC was well characterized before and after its exploitation in preparation of CQDs@Cu-BTC via SEM, EDX, XRD, FTIR analyses. The assessment was currently investigated for all of the as-prepared CQDs, Cu-BTC & CQDs@Cu-BTC as fertilizers for enhancement the morphological and physiological properties of sunflower.

2. Materials and methodology

2.1. Chemicals and materials

Copper (II) nitrate trihydrate (>99%, Sigma- Aldrich) and N,N dimethyl formamide (DMF, 99.9%, Sigma- Aldrich), benzene-1,3,5-tricarboxylic acid, (>99%, Merck) and carboxymethyl cellulose sodium salt (CMC, low viscosity, Sigma- Aldrich) were all purchased. From Sigma (St Louis, MO, USA), the standard solutions from vitamin E (α-tocopherol) & vitamin K (phylloquinone) were purchased. From Fisher (USA), all of ethanol, acetonitrile, ethanol, petroleum benzene and diethyl ether were obtained. The chemical reagents exploited for the preparation of samples were and applied as received.

2.2. Synthesis of Cu-BTC

Cu–BTC MOF was synthesized as follows; 2.077 g of tri-hydrated copper nitrate and one gram of benzene-1,3,5-tricarboxylic acid, were dissolved in 50 ml of dimethyl formamide. Then, the prepared solution was transferred for heating at 160 °C for evaporation of dimethyl formamide. The reaction liquor was left for cooling in the atmospheric air and the solidified Cu-BTC was separated with centrifugation and washed up with ethanol for 5 repeated times for the removal of the unreacted compounds. Cu-BTC was then left for drying in oven at 105 °C overnight to be in turn stored in a vacuum for further analysis and applications.

2.2.1. Synthesis of carbon quantum dots "CQDs"

Carbon quantum dots "CQDs" were nucleated from carboxymethyl cellulose "CMC" via hydrothermal technique as follows; certain concentration of NaOH (10 g/L) was added for alkaline hydrolysis of CMC (15 g/L) and subsequently the alkali-hydrolyzed carboxymethyl cellulose

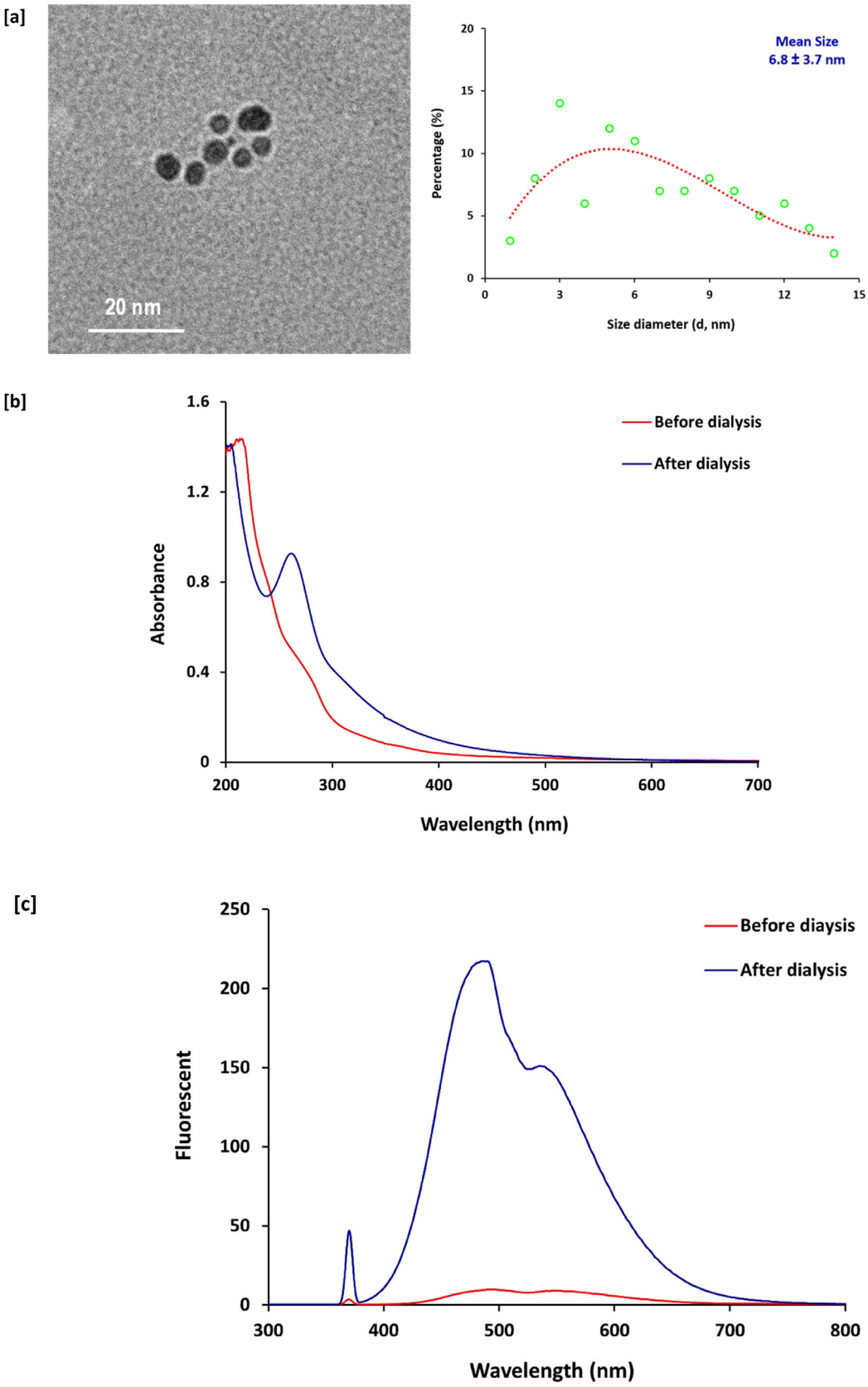

Figure 1. [a] TEM graph and particle size for the synthesized CQDs. [b, c] absorbance spectra and emission spectra (excitation at 370 nm) for CQDs and CMC.

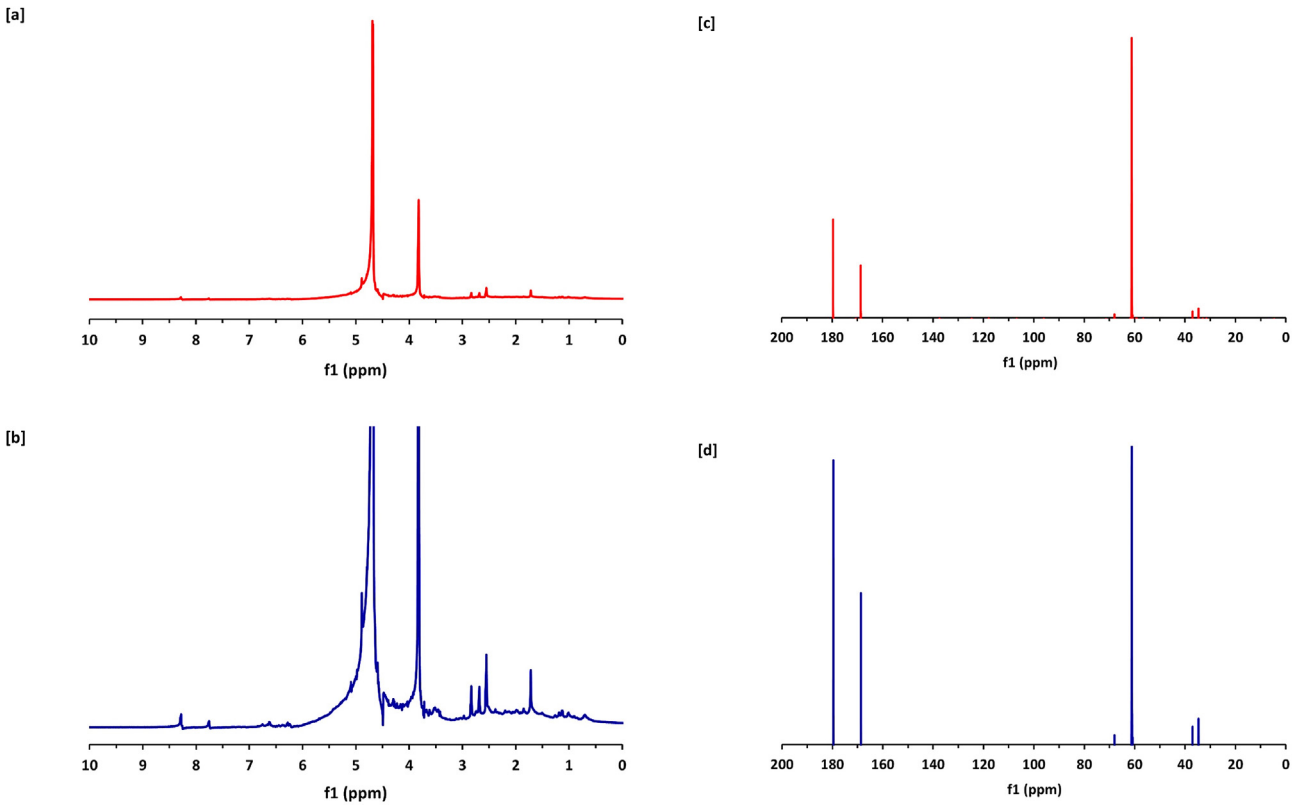

Figure 2. Spectral data for [a, c] CMC, [b, d] CQDs, [a, b] H^1NMR and [c, d] C^{13}NMR.

was left under magnetic stirring for 30 min at 90 °C. Afterwards, for complete clustering of "CQDs", the reaction liquor was transferred vertical hydrothermal autoclave reactor, then placed in an oven at 190 °C for 8 h. Lastly, the reaction liquor with darken brownish color was left for cooling in atmospheric air to be dialyzed for ultra-purification with distilled H_2O overnight using pur-A-lyzer dialysis kits (MWCO 6–8 kDa, Sigma-Aldrich).

2.2.2. Instrumental analysis

Absorption spectroscopic results for CMC and the clustered CQDs were manifested by the Cary 100 UV-VIS, from Agilent spectrophotometer. NMR spectra for CQDs were detected by the NMR spectrometer of Jeol-Ex-300 from JEOL (Japan). The chemical shifts were evaluated by ppm using TMS as the internal reference.

Topographical features and size average of the synthesized CQDs & CQDs@Cu-BTC were identified via the anticipation of HTEM (high-resolution transmission electron microscope, from Japan JEOL-JEM-1200). Size average of CQDs was calculated using 4 pi analysis software from USA" for at least 50 particles. Powder X-ray diffraction using X'Pert MPD diffractometer system from Philips was used for analyzing of CQDs, Cu-BTC & CQDs@Cu-BTC, at room temperature. Using monochromatized (Cu Kα X-radiation at 40 kV, 50 mA and $\lambda = 1.5406$ Å), the diffraction patterns were estimated in the diffraction angle (2θ) range of 3.5–50°. Infrared spectral results were detected for CQDs, Cu-BTC & CQDs@Cu-BTC using infrared Spectrometer (Jasco FT/IR 6100) conducted to detector of deuterated tri-glycine sulfate (TGS). Using transmission mode (T %), resolution of 4 cm^{-1} with 1 cm^{-1} interval scanning and scanning speed of 2 mm/s, the spectral results were measured in the range of 4000–400 cm^{-1}.

2.3. Experimental work in the field

Experimental work in the field were proceeded during 2020 seasons at the Desert Research Center (DRC) in Egypt. Experimental work was proceeded to evaluate the different effects of CQDs immobilized within MOFs on the growth of sunflowers.

2.4. Growth measurement and photosynthetic pigment measurement

Plant heights, fresh and dry weight of the whole plants were expressed as centimeter (cm) and grams (g), respectively. Dry weights were recorded after drying the plant samples in oven at 60 °C until constant weight. Chlorophyll a, b and carotenoids were extracted and estimated in fresh leaves according to [40].

2.5. Total protein content

Nitrogen protein was estimated by multiplying the total nitrogen by 6.25 [41]. Total nitrogen was determined by Kjeldahl procedure. Digestion step, oven dried plant sample 0.25 g was weighed and subjected to a high temperature digestion with concentrated H_2SO_4 and catalysts H_2O_2 to convert organic and inorganic forms of N to ammonium. Titration step, ammonium in the digest is determined by acidimetric titration following alkaline distillation of ammonia **(A.O.A.C., 1970)** and calculations were done according to [42].

2.5.1. Cultivar & Foliar applications

Cultivar Giza 102 was used in current study. It was obtained from the Field Crop Institute, Agriculture Research Center, Giza, Egypt. Control (stressed plant), CQDs, MOFs, MOFs@CQDs, Vigor Extra (as a commercial).

2.5.2. Cultivation

The pots experiment was done in a wire house at Desert Research Center (DRC) located in Cairo under saline condition (4000 ppm), during April 2020. The pots experiment (30 cm in diameter and 25 cm in height) were conducted in a warehouse at the Desert Research Center (DRC) in Cairo. The experiment was prepared as a completely randomized block

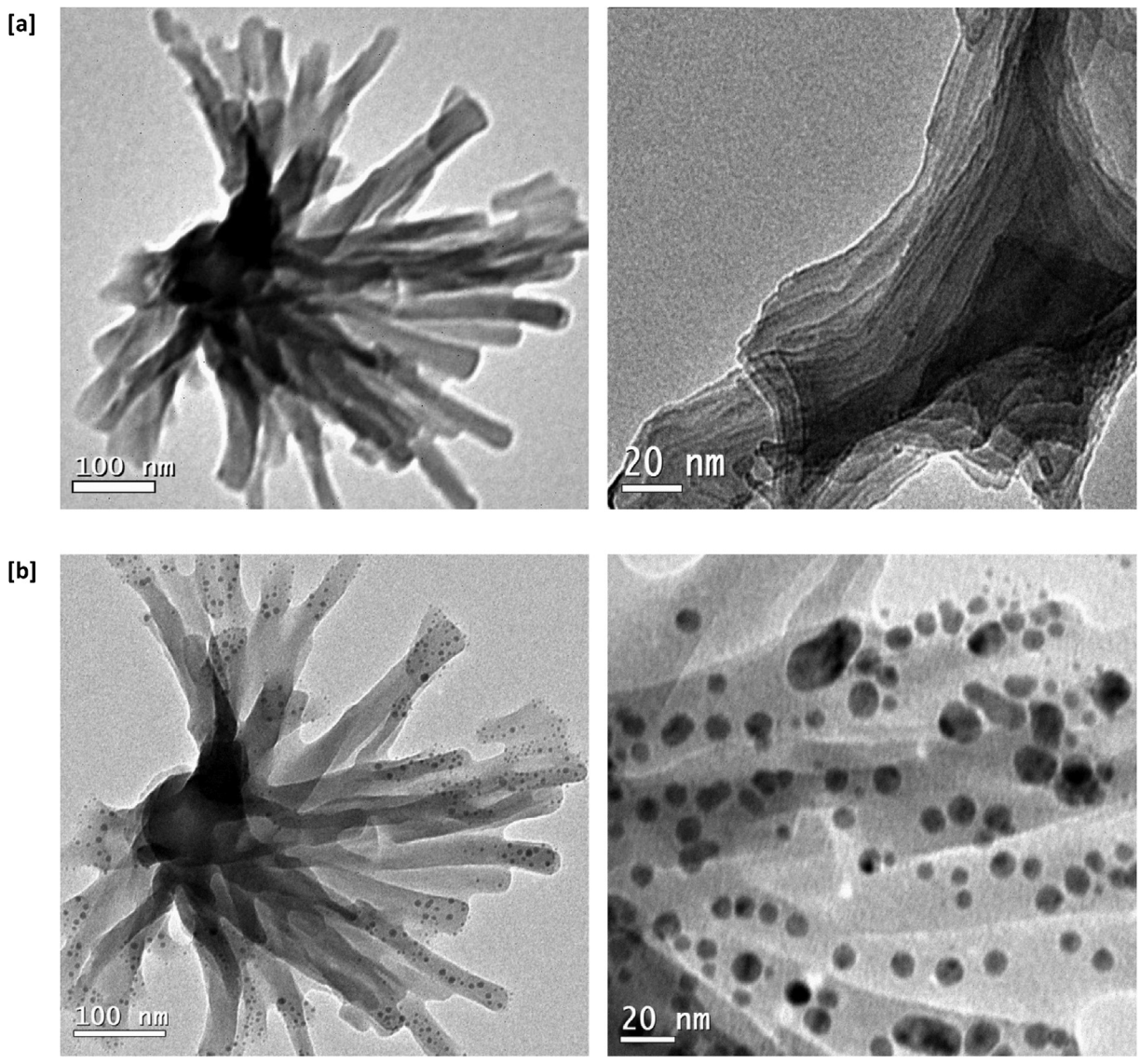

Figure 3. TEM graphs for [a] Cu-BTC and [b] CQDs@Cu-BTC.

design with four cross-controller treatments and three replicates. The filled soil was sandy loam (79.6% sand, 10.55% silt, and 9.85% clay) Huan et al. 2007 [43]. Five sunflower seeds are planted in each pot, 1.5 cm from the surface of the pot. Irrigation saline was used as a control treatment and was used with all foliar applications, salinity was determined based on the irrigation water salinity threshold given by Maas and Grattan (1999) [44]. Saline irrigation water was prepared by adding sodium chloride (NaCl) to the tap water to reach the target salinity level of the irrigation water (4000 ppm) and all the pots were irrigated with the same amount of irrigation water. The prepared irrigation water was stored in 20-liter plastic containers.

2.6. Foliar application and sampling

After 30 days from sowing, pots having similar plant growth were selected and it was sprayed with different treatments at concentration (20 ppm). Plant samples were collected after 1, 2, 4, 7, 9 and 11 days after foliar treatment. Shoots and roots were separated and determined fresh and dry weight and length. Leaves were separated to assay chlorophyll and peroxides activity.

2.7. Statistical analysis

The data were subjected to one-way ANOVA and the differences between means at the 5% probability level were determined using Duncan's new multiple range test. The software SPSS, version 16 (SPSS, Richmond, USA) was used as described by Dytham (1999) [45, 46, 47].

3. Results and discussion

3.1. Synthesis and characterization of "CQDs"

In the current approach, nucleation of "CQDs" from alkaline dissolved CMC under hydrothermal conditions was performed. According to the previously reported researches, the mechanism of reaction for "CQDs" nucleation could be predicted as CMC undergoes hydrolysis & depolymerization under strong alkaline conditions, while, under hydrothermal conditions, the alkali-fragmented residues of CMC undergo repolymerization, oxidation and aromatization, to generate graphite sheets of size/shape controllable "CQDs" decorated with oxygen containing functional groups [48, 49, 50].

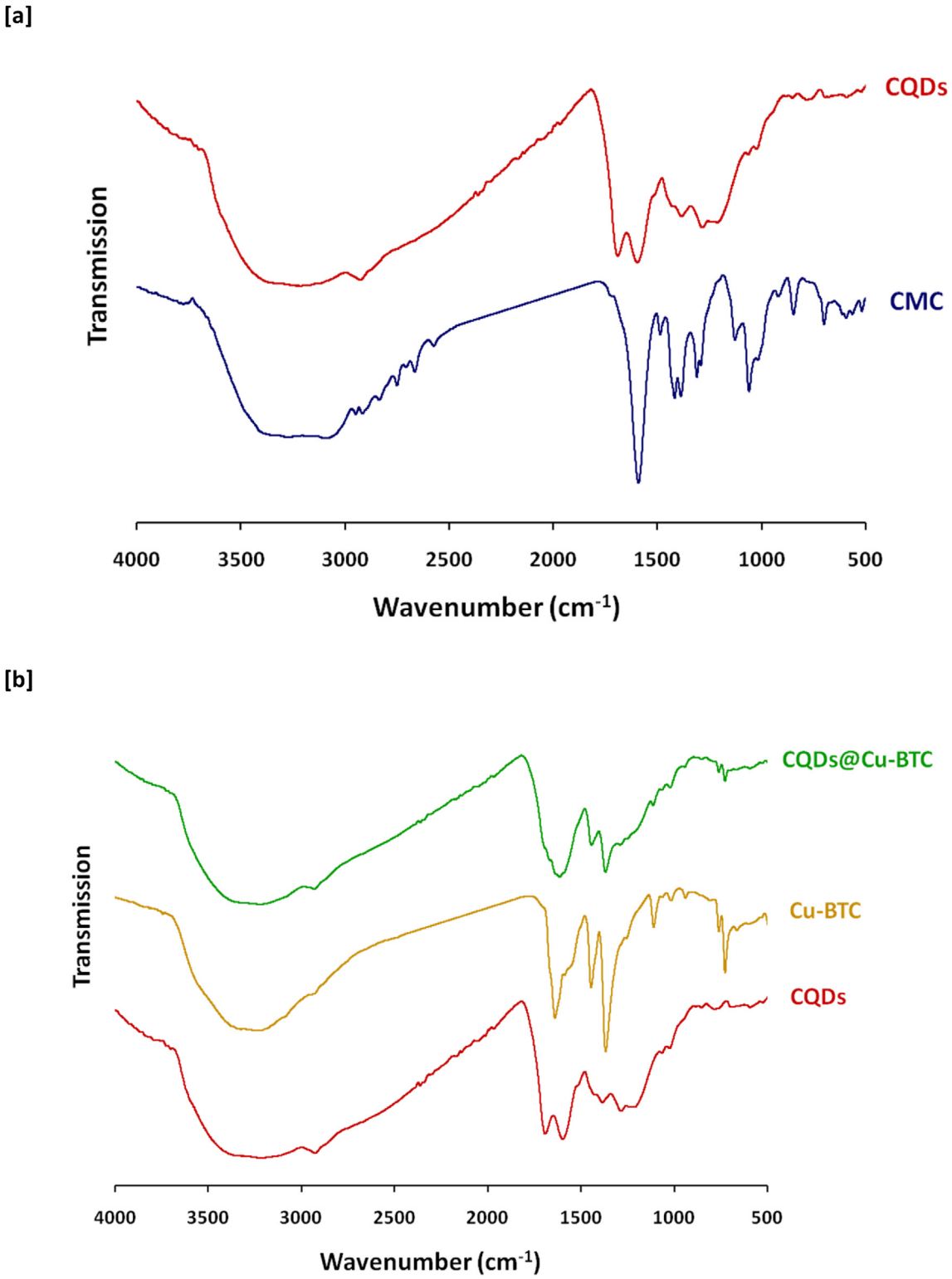

Figure 4. FTIR spectra for; [a] the synthesized CQDs and [b] CQDs@Cu-BTC.

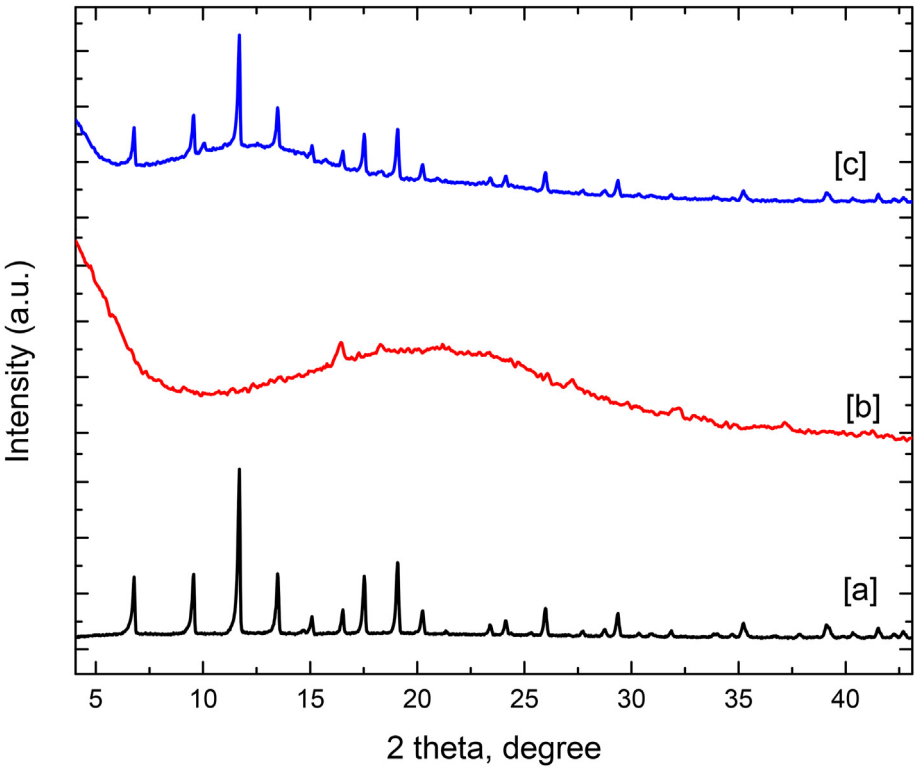

Figure 5. XRD results for [a] Cu-BTC, [b] the synthesized CQDs and [c] CQDs@Cu-BTC.

Geometry and size distribution of the nucleated "CQDs" were informed from the micrographs of Transmission Electron Microscope (TEM) (Figure 1a). TEM micrographs showed that, under hydrothermal conditions, nucleation of "CQDs" from alkali hydrolyzed CMC was successfully performed with homogenous distribution and controllably ingraining with particle size of 6.8 ± 3.7 nm.

The absorption spectroscopic analysis for "CQDs" samples prepared under hydrothermal conditons from alkali-hydrolyzed CMC was shown in Figure 1b. From the presented absorption spectral results for the nucleated "CQDs" before and after dialysis showed that, a characteristic absorption peak at 220 nm for π-π* (C=C of aromatic sp^2 bond) could be obviously detected [51, 52, 53, 54]. After dialysis, in addition to the as-mentioned peak, another absorption band was detected at 275 nm forn-π* (C=O functional groups). These could be explained in agreement with literature, as after dialysis, the byproducts and unreacted materials were eliminated to give ultra-purified/monodispersed "CQDs" [55].

The optical activity for the ingrained "CQDs" is attributed to the decorative group rather than their size distribution [55]. The surface state is described as the origin of the optical activity, resulted from the synergetic hybridization of functional group and carbon-based core [53, 56]. Therefore, the optical activity of the ingrained "CQDs" are attributed to the decorative/functional groups, with overlapping of π-π* and n-π* transitions within the graphite sheets of "CQDs". Whereas, the decorative/functional groups mainly effect on the location and intensity of the absorption band, to produce colored "CQDs".

The optical activity of the ingrained "CQDs" (excited at 370 nm) was studied via fluorescence (FL) spectroscopy and the excitation and emission spectra were presented in Figure 1c. From the plotted data, after dialysis, the emission spectra of "CQDs" ingrained from CMC showed three FL emission bands at 488 nm & 540 nm with excitation intensity of 151 and 216, respectively, which is corresponding to the yellow-green regions [57, 58, 59]. FL data could confirm that, in the current study, "CQDs" that were synthesized under the hydrothermal conditions to emit in visible region could exhibit a strong luminescence, to be superiorly exploitable in various fields.

For affirmation of the chemical composition for the hydrothermally ingrained "CQDs", ^{1}HNMR & ^{13}CNMR spectral results were analyzed and presented in Figure 2. ^{1}HNMR (Figure 2a) for CMC showed the characteristic bands for protons of O–H group and that bonded to C=O at 3.91 and 4.69 ppm, respectively. Whereas, after ingraining of "CQDs" from CMC, all of CMC characteristic bands were retained with more intense (Figure 2a). The ^{13}CNMR spectra of CMC before and after its exploitation for clustering of "CQDs" were represented in Figure 2c and d whereas, the spectral data of CMC showed the characteristic bands at 36–39 ppm and 62–74 ppm corresponding to carbon bonded to CH_2–C=O, O–CH_2, respectively, whereas, the bands at 169 ppm and 180 ppm characteristic for COO were also detected. In the same manner, after exploitation of CMC for nucleation of "CQDs" the referred characteristic bands of CMC in ^{13}CNMR spectrum were retained with more intense.

3.2. Characterization of CQDs@Cu-BTC

The geometrical features of the synthesized Cu-BTC before and after the successive impregnation of CQDs were shown via analyzing TEM micrographs (Figure 3). From the obvious observation of topography, two magnifications were analyzed. The analyzed Cu-BTC sample was observed with crystalline rod-like structure (Figure 3a). Additionally, Figure 3b showed that, CQDs that were formerly ingrained from CMC macromolecules are well distributed/successfully impregnated within Cu-BTC matrix (Figure 3b).

FT-IR spectral analyses for CMC, CQDs and CQDs@Cu-BTC were plotted in Figure 4. From Figure 4a it could be depicted that; the spectrum of CMC has typical bands at 3318 cm^{-1} and 2926 cm^{-1} for O–H group and –CH_2 aliphatic carbon, respectively. In addition to, characteristic bands at 1602 cm^{-1}, 1433 cm^{-1}, 1371 cm^{-1}, 1067 cm^{-1} and 856 cm^{-1}, corresponding to carbonyl group, –CH_2 asymmetric, C–C aliphatic

Figure 6. Photos of sunflower plant after seeding; [a] using commercial nutrient, [b] using Cu-BTC, [c] using CQDs, [d] using CQDs@Cu-BTC and [f] collect images for all nutrient.

chain vibration, glycoside bond between monomers of CMC and pyranose rings, respectively. FT-IR spectra for "CQDs" were shown with significant difference from that of CMC, to approve the successive clustering of "CQDs" from CMC polymeric matrix. It can be obviously observed that, the characteristic bands of CMC were fully disappeared and the characteristic peak for C=C stretch aromatic was newly observed at 1708–1620 cm^{-1}. A significant band characteristic for C–C aromatic ring chain vibration was estimated at 1360–1050 cm^{-1} (Figure 4b). Cu-BTC showed four significant transmission bands at 3368, 1650/1602, 1453, 1374 and 733 cm^{-1}. These bands are characterized for O–H, O–C=O, C=C, C–O and Cu–O, respectively [60, 61, 62]. After anchoring of CQDs within Cu–BTC framework, a broad peak was detected at 1763 cm^{-1} which is resulted from the overlapping between O–C=O group of butane tetra-carboxylic acid (BTC) and C=C aromatic of CQDs. This could affirm the successive encaging of CQDs within Cu-BTC framework via the chemical interaction between Cu–BTC and CQDs via COOH and OH groups of CQDs and copper as a metallic center of Cu-BTC [63, 64, 65].

Moreover, XRD analyses were presented in Figure 5 for Cu–BTC, CQDs and CQDs@Cu–BTC. The figured-out data showed that, CQDs were signified with a broad peak at $2\theta = 20°$ which is indicated for the amorphous structure of CQDs [66, 67, 68]. For Cu–BTC, different peaks at $2\theta = 6.8°$, 9.5°, 11.6°, 13.4°, 17.5°, 19.2°, 20.2°, 26.0°, 29.5°, 35.2°and 39.1° were estimated and were corresponding to PXRD data of

Cu–BTC that were previously reported in literature [69, 70, 71]. The characteristic diffraction peaks of CQDs and Cu–BTC were both detected for CQDs@Cu–BTC at the same diffraction angle. This could affirm that encaging of CQDs within Cu–BTC framework did not significantly effect on the crystalline structure of Cu–BTC.

3.3. Application of CQDs, Cu-BTC & CQDs@Cu-BTC in sunflower nourishment

Sunflower (*Helianthus annuus, L.*) is one of the important oil crops, belonging to Asteraceae (Compositae) family, genus Helianthus. Attributing to its high adaptability for different stresses, its productivity is non-significantly affected by the photoperiod and altitude [72]. Herein the effects of CQDs, Cu-BTC & CQDs@Cu-BTC for enhancement the morphological and physiological properties of sunflower were investigated.

3.4. Physiological properties

Monitoring the interchanging for the amounts of chlorophylls and carotenoids as the most essential photosynthetic pigments are known as a type of the physiological parameters for monitoring the plant growth [73]. The amounts of the chlorophyll per unit leaf area are key parameter for the growth rate of any studied plant. Wu et al. [74] and Hawkins et al. [75], were reported that, estimation of chlorophyll content could be useful for the detection and following up the photosynthetic activity, the status of nutrition, and physiological changing of the plants.

Figure 6 (a–e) represented the photos of sunflower plant after seeding under the effects of commercial nutrient, Cu-BTC, CQDs, and CQDs@Cu-BTC, as it could be obviously observed the superior effects of Cu-BTC, CQDs, and CQDs@Cu-BTC compared to the commercial nutrient in the growth rate of the tested plant. Figure 7 and Table S1 (supplementary data) were represented the estimated contents of photosynthetic pigments (chlorophyll a, chlorophyll b and carotenoids) over 12 days Figure 7(a–c). The variance analysis reveals significant effects of all the prepared CQDs, Cu-BTC & CQDs@Cu-BTC on chlorophyll a and b and carotenoids levels. They were shown the following order for the increment of the of photosynthetic pigments contents; commercial nutrient < CQDs < Cu-BTC < CQDs@Cu-BTC. The CQDs@Cu-BTC composite showed the superior affinity for increment the photosynthetic pigments contents. From the estimated data, after 12 days from seeding, the contents of chlorophyll a, chlorophyll b and carotenoids were estimated for sunflower sample that was fed with CQDs to be 0.465 ± 0.001 mg/g, 0.393 ± 0.004 mg/g and 0.350 ± 0.001 mg/g, whereas, that fed with CQDs@Cu-BTC was estimated with 0.497 ± 0.002 mg/g, 0.412 ± 0.002 mg/g and 0.364 ± 0.0003 mg/g, respectively.

3.5. Morphological properties

As the shoot acts in supplying water and nutrients from root to the rest of the plant, the shoot length is one of the most important morphological parameters for monitoring the plant growing rate. Similarly, elongation of root also gives an indication for the rate of the plant growth, whereas, root system is essential for supporting the plant with water and minerals deeply form the soil. Figure 8(a,b) and (Table S2 & S3 in supplementary data) were shown the effect of feeding sunflower samples with the as-prepared CQDs, Cu-BTC & CQDs@Cu-BTC on shoot length. The estimated data showed that, elongation of shoot and root was observably detected by feeding the sunflower samples with all of the prepared CQDs, Cu-BTC & CQDs@Cu-BTC. However, CQDs@Cu-BTC was exhibited with the highest affinity in improving the shoot and root lengths. After 12 days from seeding, the shoot length was estimated for sunflower sample that was treated with CQDs to be 38.7 ± 0.33, whereas, that fed with CQDs@Cu-BTC was estimated with 46.5 ± 0.29. Additionally, the root

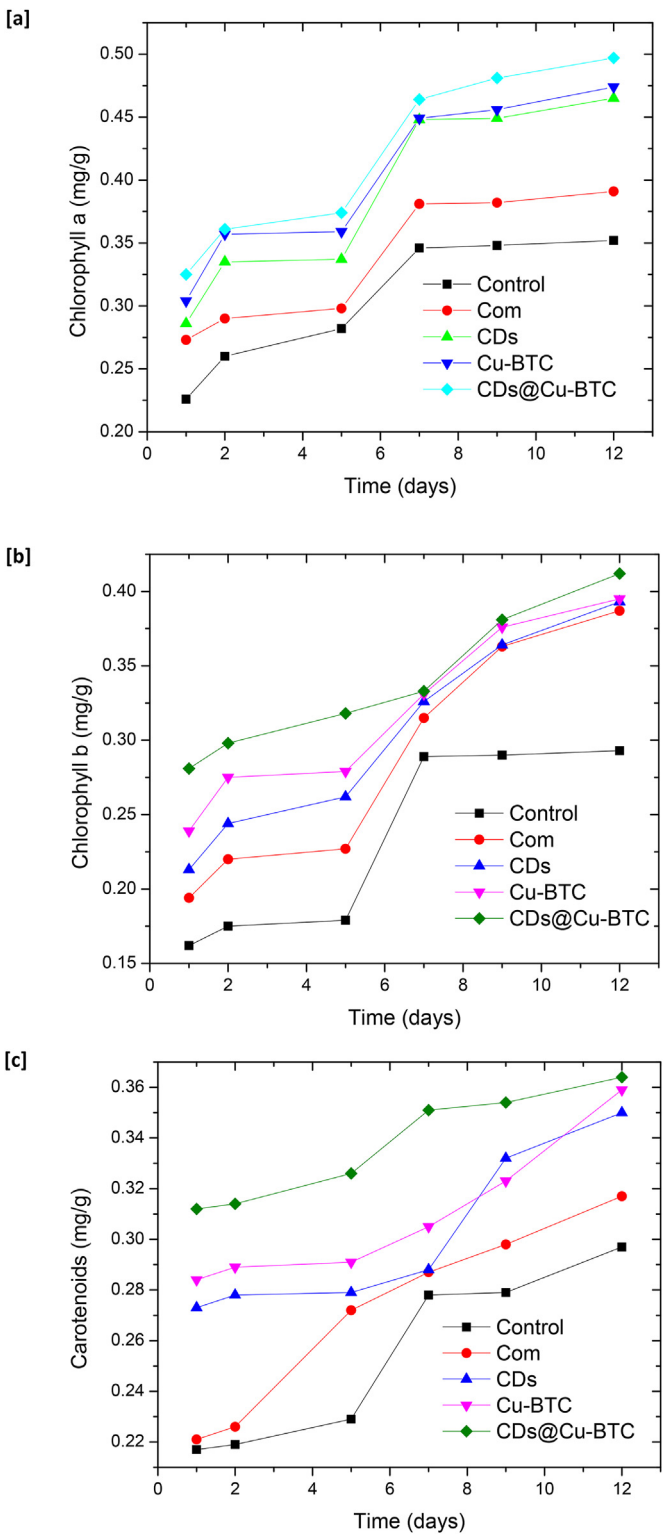

Figure 7. The extracted photosynthetic pigments from leaves of sunflower; [a] chlorophyl a, [b] chlorophyl b, and [c] carotenoids.

length was evaluated for sunflower sample that was fertilized with CQDs to be 8.3 ± 0.17, while, that treated with CQDs@Cu-BTC was shown with root length values 9.5 ± 0.29.

The effect of sunflower nourishment with the synthesized CQDs, Cu-BTC & CQDs@Cu-BTC on both of shoot dry and fresh weights and root

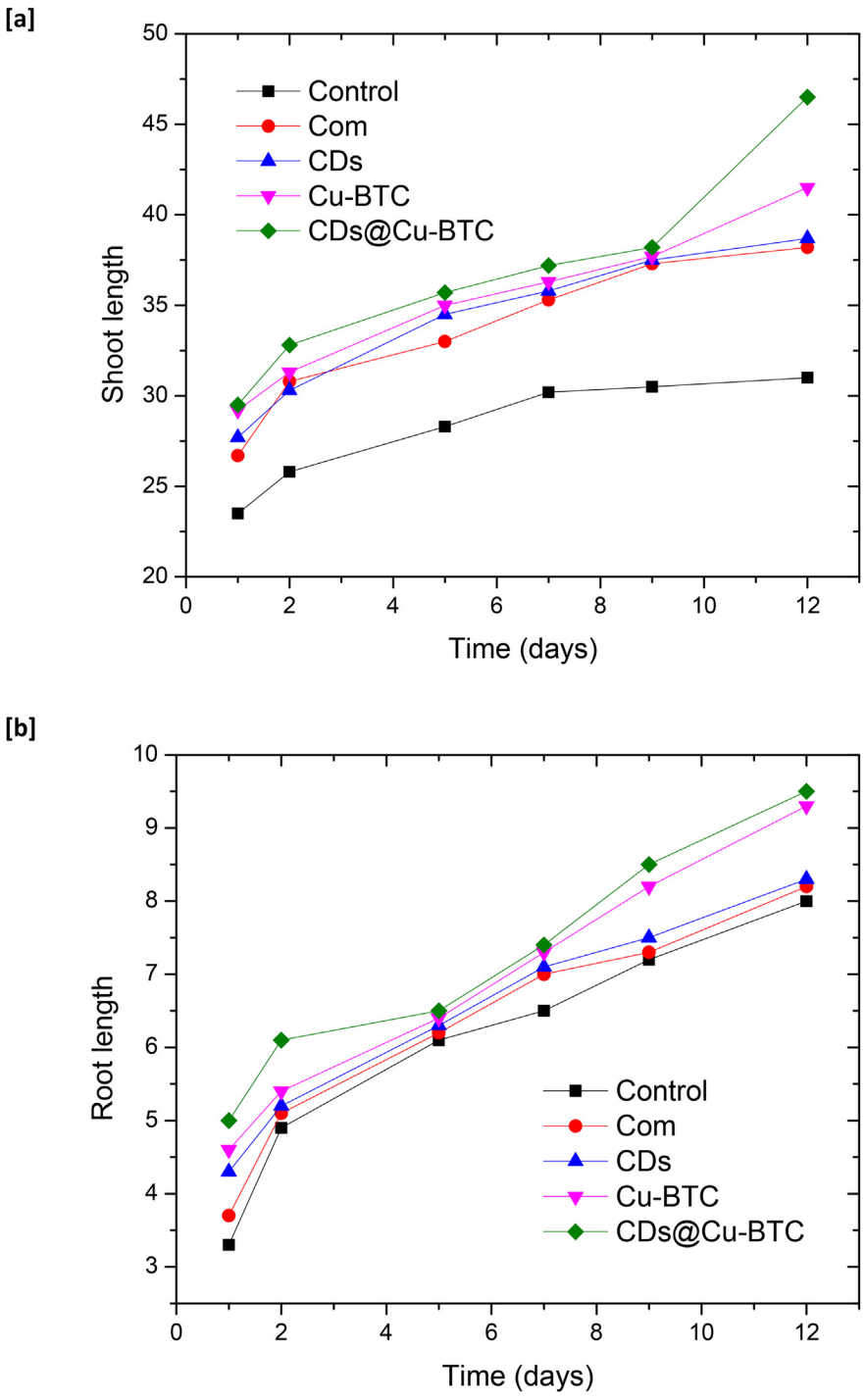

Figure 8. Effect of foliar applications on germination of sunflower; [a] shoot length, [b] root length.

dry and fresh weights were also estimated as displayed in Figure 9(a–d) and (Tables S4, S5, S6, S7 in supplementary data). The CQDs@Cu-BTC composite exhibited with highest efficiency for increment the root and shoot weights. After 12 days, the shoot fresh weight was estimated for sunflower sample that was grown under the effect of CQDs to be 2.64 ± 0.02 (shoot dry weight, 0.27 ± 0.00), whereas, that fed with CQDs@Cu-BTC was evaluated with shoot fresh weight of 3.23 ± 0.02 (shoot dry weight, 0.37 ± 0.00). On the other hand, the root fresh weight was estimated for sunflower sample that was exposed to CQDs for growing to be 0.37 ± 0.00 (root dry weight, 0.055 ± 0.00). While, feeding with CQDs@Cu-BTC exhibited root fresh weight of 0.47 ± 0.00 (root dry weight, 0.063 ± 0.001). Similarly, the trend for, shoot and root elongation and increment the shoot and root weights (even dry or fresh weights) was as follows; commercial nutrient < CQDs < Cu-BTC < CQDs@Cu-BTC, that is in harmony with the estimated data of physiological parameters.

4. Conclusion

The present study focused on the successful application of CQDs@Cu-BTC composite as fertilizer for the sunflower to enhance the photosynthetic activity, the status of nutrition, and physiological changing. CQDs were hydrothermally synthesized from CMC with size of 6.8 nm and then anchored within Cu-BTC forming CQDs@Cu-BTC composite. The

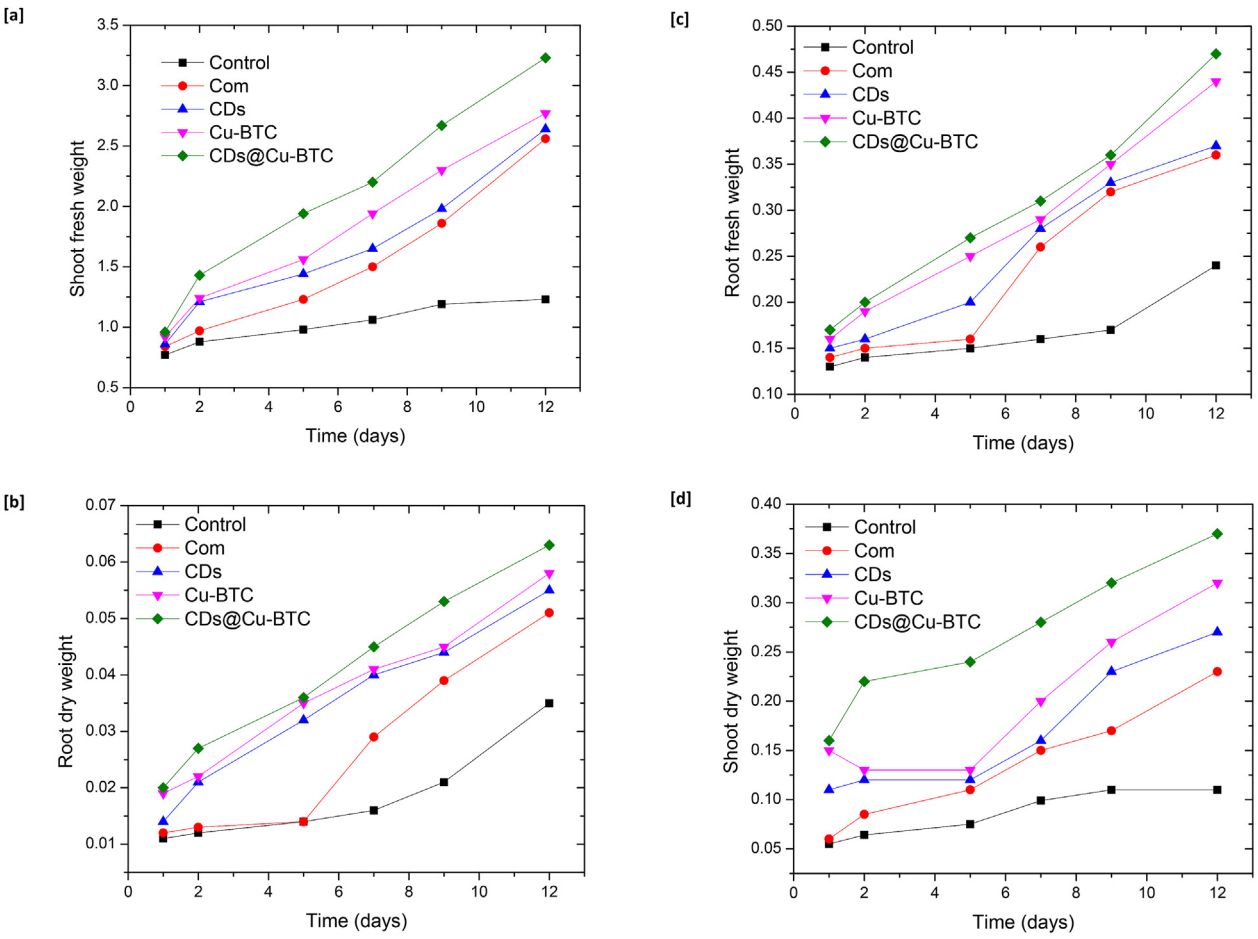

Figure 9. Effect of foliar applications on germination of sunflower; [a] shoot fresh weight, [b]shoot dry length, [c] root fresh weight and [d] root dry weight.

synthesized CQDs were characterized by UV-visible, TEM, NMR, FTIR and XRD. The assessment for CQDs and CQDs@Cu-BTC as fertilizers for sunflower was subsequently investigated. The variance analysis reveals significant effects of all the applied CQDs materials on chlorophyll a and b and carotenoids levels, the shoot & root elongation and the shoot & root weights (dry or fresh). They were shown the following order for the increment of photosynthetic pigments contents and long & weight of sunflower; commercial nutrient < CQDs < Cu-BTC < CQDs@Cu-BTC. After feeding with CQDs & CQDs@Cu-BTC, the contents of chlorophyll a and carotenoids were 0.465 & 0.497 mg/g and 0.350 & 0.364 mg/g, respectively. While, the length of sunflower shoot was 38.7 cm and 46.5 cm after treatment with CQDs and CQDs@Cu-BTC, respectively. The results showed that the application of CQDs@Cu-BTC as fertilizer superiorly enhanced the growth and the photosynthetic pigments contents of sunflower and subsequently could be applicable as a plant fertilizer instead of the commercial nutrient. The current study will open the way for exploiting of CQDs separately or in combination with other materials as nutrient for plants and substituent for the hazardous fertilizers.

Declarations

Author contribution statement

Hanan B. Ahmed: Analyzed and interpreted the data; Contributed reagents, materials, analysis tools or data; Wrote the paper.

Noura E. Mahmoud; Asmaa A. Mahdi: Conceived and designed the experiments; Performed the experiments.

Hossam E. Emam: Conceived and designed the experiments; Analyzed and interpreted the data; Contributed reagents, materials, analysis tools or data; Wrote the paper.

Reda M. Abdelhameed: Conceived and designed the experiments; Analyzed and interpreted the data; Contributed reagents, materials, analysis tools or data.

Funding statement

This research did not receive any specific grant from funding agencies in the public, commercial, or not-for-profit sectors.

Data availability statement

Data will be made available on request.

Declaration of interest's statement

The authors declare no conflict of interest.

Additional information

Supplementary content related to this article has been published online at https://doi.org/10.1016/j.heliyon.2022.e12396.

References

[1] S. Mazaherinia, A.R. Astaraei, A. Fotovat, A. Monshi, Nano iron oxide particles efficiency on Fe, Mn, Zn and Cu concentrations in wheat plant, World Appl. Sci. J. 7 (2010) 36–40.

[2] K. Chaudhary, K. Prakash, D.T. Masram, TiO2 nanoparticles immobilized organo-reduced graphene oxide hybrid nanoreactor for catalytic applications, Appl. Surf. Sci. 509 (2020), 144902.

[3] K. Prakash Subodh, D.T. Masram, Silver nanoparticles immobilized covalent organic microspheres for hydrogenation of nitroaromatics with intriguing catalytic activity, ACS Appl. Polym. Mater. 3 (1) (2020) 310–318.

[4] D. Yadav, S.K. Awasthi, A Pd NP-confined novel covalent organic polymer for catalytic applications, New J. Chem. 44 (4) (2020) 1320–1325.

[5] H.E. Emam, H.B. Ahmed, R.M. Abdelhameed, Melt intercalation technique for synthesis of hetero-metallic@ chitin bio-composite as recyclable catalyst for prothiofos hydrolysis, Carbohydr. Polym. 266 (2021), 118163.

[6] H.E. Emam, M.M. Mikhail, S. El-Sherbiny, K.S. Nagy, H.B. Ahmed, Metal-dependent nano-catalysis in reduction of aromatic pollutants, Environ. Sci. Pollut. Control Ser. 27 (6) (2020) 6459–6475.

[7] M. Premanathan, K. Karthikeyan, K. Jeyasubramanian, G. Manivannan, Selective toxicity of ZnO nanoparticles toward Gram-positive bacteria and cancer cells by apoptosis through lipid peroxidation, Nanomed. Nanotechnol. Biol. Med. 7 (2) (2011) 184–192.

[8] S.S. Mukhopadhyay, Nanotechnology in agriculture: prospects and constraints, Nanotechnol. Sci. Appl. 7 (2014) 63.

[9] P.K. Srivastava, V.P. Singh, A. Singh, D.K. Tripathi, S. Singh, S.M. Prasad, D.K. Chauhan, Pesticides in Crop Production: Physiological and Biochemical Action, John Wiley & Sons, 2020, pp. 221–231.

[10] C.C. Castañeda-Murillo, J.G. Rojas-Ortiz, A.D. Sánchez-Reinoso, C.C. Chávez-Arias, H. Restrepo-Díaz, Foliar brassinosteroid analogue (DI-31) sprays increase drought tolerance by improving plant growth and photosynthetic efficiency in lulo plants, Heliyon 8 (2) (2022), e08977.

[11] H. Zhu, J. Han, J.Q. Xiao, Y. Jin, Uptake, translocation, and accumulation of manufactured iron oxide nanoparticles by pumpkin plants, J. Environ. Monit. 10 (6) (2008) 713–717.

[12] M.C. DeRosa, C. Monreal, M. Schnitzer, R. Walsh, Y. Sultan, Nanotechnology in fertilizers, Nat. Nanotechnol. 5 (2) (2010) 91.

[13] M. Naderi, A. Danesh-Shahraki, Nanofertilizers and their roles in sustainable agriculture, Intl. J. Agric. Crop Sci. 5 (19) (2013) 2229–2232.

[14] R. Liu, R. Lal, Potentials of engineered nanoparticles as fertilizers for increasing agronomic productions, Sci. Total Environ. 514 (2015) 131–139.

[15] S.Y. Lim, W. Shen, Z. Gao, Carbon quantum dots and their applications, Chem. Soc. Rev. 44 (1) (2015) 362–381.

[16] R. Jalili, M. Amjadi, Bio-inspired molecularly imprinted polymer–green emitting carbon dot composite for selective and sensitive detection of 3-nitrotyrosine as a biomarker, Sensor. Actuator. B Chem. 255 (2018) 1072–1078.

[17] R. Atchudan, T.N.J.I. Edison, S. Perumal, R. Vinodh, Y.R. Lee, In-situ green synthesis of nitrogen-doped carbon dots for bioimaging and TiO2 nanoparticles@ nitrogen-doped carbon composite for photocatalytic degradation of organic pollutants, J. Alloys Compd. 766 (2018) 12–24.

[18] R. Atchudan, T.N.J.I. Edison, Y.R. Lee, Nitrogen-doped carbon dots originating from unripe peach for fluorescent bioimaging and electrocatalytic oxygen reduction reaction, J. Colloid Interface Sci. 482 (2016) 8–18.

[19] T.N.J.I. Edison, R. Atchudan, M.G. Sethuraman, J.-J. Shim, Y.R. Lee, Microwave assisted green synthesis of fluorescent N-doped carbon dots: cytotoxicity and bio-imaging applications, J. Photochem. Photobiol. B Biol. 161 (2016) 154–161.

[20] J. Zhao, M. Huang, L. Zhang, M. Zou, D. Chen, Y. Huang, S. Zhao, Unique approach to develop carbon dot-based nanohybrid near-infrared ratiometric fluorescent sensor for the detection of mercury ions, Anal. Chem. 89 (15) (2017) 8044–8049.

[21] W. Wu, L. Zhan, W. Fan, J. Song, X. Li, Z. Li, R. Wang, J. Zhang, J. Zheng, M. Wu, Cu–N dopants boost electron transfer and photooxidation reactions of carbon dots, Angew. Chem. Int. Ed. 54 (22) (2015) 6540–6544.

[22] Z. Tian, X. Zhang, D. Li, D. Zhou, P. Jing, D. Shen, S. Qu, R. Zboril, A.L. Rogach, Full-color inorganic carbon dot phosphors for white-light-emitting diodes, Adv. Opt. Mater. 5 (19) (2017), 1700416.

[23] Y. Zhou, D. Benetti, X. Tong, L. Jin, Z.M. Wang, D. Ma, H. Zhao, F. Rosei, Colloidal carbon dots based highly stable luminescent solar concentrators, Nano Energy 44 (2018) 378–387.

[24] S. Qu, X. Wang, Q. Lu, X. Liu, L. Wang, A biocompatible fluorescent ink based on water-soluble luminescent carbon nanodots, Angew. Chem., Int. Ed. 51 (49) (2012) 12215–12218.

[25] D. Pooja, S. Saini, A. Thakur, B. Kumar, S. Tyagi, M.K. Nayak, A "Turn-On" thiol functionalized fluorescent carbon quantum dot based chemosensory system for arsenite detection, J. Hazard Mater. 328 (2017) 117–126.

[26] H. Wang, M. Zhang, Y. Song, H. Li, H. Huang, M. Shao, Y. Liu, Z. Kang, Carbon dots promote the growth and photosynthesis of mung bean sprouts, Carbon 136 (2018) 94–102.

[27] L.-X. Su, X.-L. Ma, K.-K. Zhao, C.-L. Shen, Q. Lou, D.-M. Yin, C.-X. Shan, Carbon nanodots for enhancing the stress resistance of peanut plants, ACS Omega 3 (12) (2018) 17770–17777.

[28] H. Li, J. Huang, F. Lu, Y. Liu, Y. Song, Y. Sun, J. Zhong, H. Huang, Y. Wang, S. Li, Impacts of carbon dots on rice plants: boosting the growth and improving the disease resistance, ACS Appl. Bio Mater. 1 (3) (2018) 663–672.

[29] S.H. Schwartz, B. Hendrix, P. Hoffer, R.A. Sanders, W. Zheng, Carbon Dots for Efficient siRNA Delivery and Gene Silencing in Plants, 2019, 722595 bioRxiv.

[30] Z. Yao, Z. Lai, C. Chen, S. Xiao, P. Yang, Full-color emissive carbon-dots targeting cell walls of onion for in situ imaging of heavy metal pollution, Analyst 144 (11) (2019) 3685–3690.

[31] M. Anstoetz, T.J. Rose, M.W. Clark, L.H. Yee, C.A. Raymond, T. Vancov, Novel applications for oxalate-phosphate-amine metal-organic-frameworks (OPA-MOFs): can an iron-based OPA-MOF be used as slow-release fertilizer? PLoS One 10 (12) (2015), e0144169.

[32] M. Anstoetz, N. Sharma, M. Clark, L.H. Yee, Characterization of an oxalate-phosphate-amine metal–organic framework (OPA-MOF) exhibiting properties suited for innovative applications in agriculture, J. Mater. Sci. 51 (20) (2016) 9239–9252.

[33] R.M. Abdelhameed, R.E. Abdelhameed, H.A. Kamel, Iron-based metal-organic-frameworks as fertilizers for hydroponically grown Phaseolus vulgaris, Mater. Lett. 237 (2019) 72–79.

[34] G. Certini, G. Corti, F.C. Ugolini, Vertical trends of oxalate concentration in two soils under Abies alba from Tuscany (Italy), J. Plant Nutr. Soil Sci. 163 (2) (2000) 173–177.

[35] G. Cailleau, O. Braissant, E. Verrecchia, Turning sunlight into stone: the oxalate-carbonate pathway in a tropical tree ecosystem, Biogeosciences 8 (7) (2011) 1755–1767.

[36] G. Cailleau, M. Mota, S. Bindschedler, P. Junier, E.P. Verrecchia, Detection of active oxalate–carbonate pathway ecosystems in the Amazon Basin: global implications of a natural potential C sink, Catena 116 (2014) 132–141.

[37] J.M. Rivera, S. Rincón, C. Ben Youssef, A. Zepeda, Highly efficient adsorption of aqueous Pb (II) with mesoporous metal-organic framework-5: an equilibrium and kinetic study, J. Nanomater. (2016). Article ID 8095737.

[38] N. Mahadi, H. Misran, S. Othman, A. Manap, M. Salim, N. Shah, N. Razak, N. Anuar, Low-cost Synthesis and Characterizations of Metal-Organic Framework (MOF-199) Materials by Nonsurfactant Templating Method, Advanced Materials Research, Trans Tech Publ, 2015, pp. 426–429.

[39] Y.-R. Lee, J. Kim, W.-S. Ahn, Synthesis of metal-organic frameworks: a mini review, Kor. J. Chem. Eng. 30 (9) (2013) 1667–1680.

[40] W. Horwitz, P. Chichilo, H. Reynolds, Official Methods of Analysis of the Association of Official Analytical Chemists, Official methods of analysis of the Association of Official Analytical Chemists, Washington, 1970.

[41] Aoac, Association of official analytical chemists, Official Methods of Analysis, AOAC, Arlington, VA, USA, 1990.

[42] A. Magomya, D. Kubmarawa, J. Ndahi, G. Yebpella, Determination of plant proteins via the kjeldahl method and amino acid analysis: a comparative study, Int. J. Sci. Technol. Res. 3 (4) (2014) 68–72.

[43] H. Huan, J. Zhou, Z. Duan, H. Wang, Y. Gao, Contributions of greenhouse soil nutrients accumulation to the formation of the secondary salinization: a case study of Yixing city, China, Agrochimica 51 (4-5) (2007) 207–221.

[44] E.V. Maas, S. Grattan, Crop yields as affected by salinity, Agric. Drain. 38 (1999) 55–108.

[45] C. Dytham, Choosing and Using Statistics: A Biologist's Guide, John Wiley & Sons, 2011.

[46] P. Nguyen, B. Reynolds, J. Zentek, N. Paßlack, V. Leray, Sodium in feline nutrition, J. Anim. Physiol. Anim. Nutr. 101 (2017) 403.

[47] R.S. Kuntal, R. Gupta, D. Rajendran, V. Patil, Study of Real-Coded Hybrid Genetic Algorithm (Rga) to Find Least-Cost Ration for Non-pregnant Dairy Buffaloes, Soft Computing for Problem Solving, Springer, 2019, pp. 369–389.

[48] H. Li, H. Ming, Y. Liu, H. Yu, X. He, H. Huang, K. Pan, Z. Kang, S.-T. Lee, Fluorescent carbon nanoparticles: electrochemical synthesis and their pH sensitive photoluminescence properties, New J. Chem. 35 (11) (2011) 2666–2670.

[49] T. Sakaki, M. Shibata, T. Miki, H. Hirosue, N. Hayashi, Reaction model of cellulose decomposition in near-critical water and fermentation of products, Bioresour. Technol. 58 (2) (1996) 197–202.

[50] B. Chen, F. Li, S. Li, W. Weng, H. Guo, T. Guo, X. Zhang, Y. Chen, T. Huang, X. Hong, Large scale synthesis of photoluminescent carbon nanodots and their application for bioimaging, Nanoscale 5 (5) (2013) 1967–1971.

[51] C. Kim, T. Ji, J.B. Eom, Determination of organic compounds in water using ultraviolet LED, Meas. Sci. Technol. 29 (4) (2018), 045802.

[52] Y.J. Kim, P. Guo, R.D. Schaller, Aqueous carbon quantum dot-embedded PC60-PC61BM nanospheres for ecological fluorescent printing: contrasting fluorescence resonance energy-transfer signals between watermelon-like and random morphologies, J. Phys. Chem. Lett. 10 (21) (2019) 6525–6535.

[53] Z. Luo, Y. Lu, L.A. Somers, A.C. Johnson, High yield preparation of macroscopic graphene oxide membranes, J. Am. Chem. Soc. 131 (3) (2009) 898–899.

[54] Z.L. Wu, M.X. Gao, T.T. Wang, X.Y. Wan, L.L. Zheng, C.Z. Huang, A general quantitative pH sensor developed with dicyandiamide N-doped high quantum yield graphene quantum dots, Nanoscale 6 (7) (2014) 3868–3874.

[55] X. Gao, C. Du, Z. Zhuang, W. Chen, Carbon quantum dot-based nanoprobes for metal ion detection, J. Mater. Chem. C 4 (29) (2016) 6927–6945.

[56] B. Zhang, C.y. Liu, Y. Liu, A novel one-step approach to synthesize fluorescent carbon nanoparticles, Eur. J. Inorg. Chem. 2010 (28) (2010) 4411–4414.

[57] S.P. Sasikala, L. Henry, G. Yesilbag Tonga, K. Huang, R. Das, B. Giroire, S. Marre, V.M. Rotello, A. Penicaud, P. Poulin, High yield synthesis of aspect ratio controlled graphenic materials from anthracite coal in supercritical fluids, ACS Nano 10 (5) (2016) 5293–5303.

[58] M. Li, C. Yu, C. Hu, W. Yang, C. Zhao, S. Wang, M. Zhang, J. Zhao, X. Wang, J. Qiu, Solvothermal conversion of coal into nitrogen-doped carbon dots with singlet oxygen generation and high quantum yield, Chem. Eng. J. 320 (2017) 570–575.

[59] Y.T. Yew, A.H. Loo, Z. Sofer, K. Klímová, M. Pumera, Coke-derived graphene quantum dots as fluorescence nanoquencher in DNA detection, Appl. Mater. Today 7 (2017) 138–143.

[60] C. Cai, X. Fan, X. Han, J. Li, H. Vardhan, Improved desulfurization performance of polyethyleneglycol membrane by incorporating metal organic framework CuBTC, Polymers 12 (2) (2020) 414.

[61] Y. Li, J. Miao, X. Sun, J. Xiao, Y. Li, H. Wang, Q. Xia, Z. Li, Mechanochemical synthesis of Cu-BTC@ GO with enhanced water stability and toluene adsorption capacity, Chem. Eng. J. 298 (2016) 191–197.

[62] T. Noor, M. Ammad, N. Zaman, N. Iqbal, L. Yaqoob, H. Nasir, A highly efficient and stable copper BTC metal organic framework derived electrocatalyst for oxidation of methanol in DMFC application, Catal. Lett. 149 (12) (2019) 3312–3327.

[63] R.M. Abdelhameed, M. El-Shahat, H.E. Emam, Employable metal (Ag & Pd)@ MIL-125-NH2@ cellulose acetate film for visible-light driven photocatalysis for reduction of nitro-aromatics, Carbohydr. Polym. 247 (2020), 116695.
[64] H.E. Emam, o.m. darwesh, R.M. Abdelhameed, Protective cotton textiles via amalgamation of cross-linked zeolitic imidazole framework, Ind. Eng. Chem. Res. 59 (23) (2020) 10931–10944.
[65] H.E. Emam, T. Bechtold, Cotton fabrics with UV blocking properties through metal salts deposition, Appl. Surf. Sci. 357 (2015) 1878–1889.
[66] L. Zhao, H. Li, Y. Xu, H. Liu, T. Zhou, N. Huang, Y. Li, L. Ding, Selective detection of copper ion in complex real samples based on nitrogen-doped carbon quantum dots, Anal. Bioanal. Chem. 410 (18) (2018) 4301–4309.
[67] H.B. Ahmed, H.E. Emam, Environmentally exploitable biocide/fluorescent metal marker carbon quantum dots, RSC Adv. 10 (70) (2020) 42916–42929.
[68] H.E. Emam, H.B. Ahmed, Antitumor/antiviral carbon quantum dots based on carrageenan and pullulan, Int. J. Biol. Macromol. 170 (2021) 688–700.
[69] S.S.-Y. Chui, S.M.-F. Lo, J.P. Charmant, A.G. Orpen, I.D. Williams, A chemically functionalizable nanoporous material $[Cu_3(TMA)_2(H_2O)_3]_n$, Science 283 (5405) (1999) 1148–1150.
[70] B. Xiao, P.S. Wheatley, X. Zhao, A.J. Fletcher, S. Fox, A.G. Rossi, I.L. Megson, S. Bordiga, L. Regli, K.M. Thomas, High-capacity hydrogen and nitric oxide adsorption and storage in a metal− organic framework, J. Am. Chem. Soc. 129 (5) (2007) 1203–1209.
[71] R.M. Abdelhameed, H. Abdel-Gawad, M. Elshahat, H.E. Emam, Cu–BTC@ cotton composite: design and removal of ethion insecticide from water, RSC Adv. 6 (48) (2016) 42324–42333.
[72] L. Souza, W.A. Bunn, J.F. Weltzin, N.J. Sanders, Similar biotic factors affect early establishment and abundance of an invasive plant species across spatial scales, Biol. Invasions 13 (1) (2011) 255–267.
[73] F. Silla, A. González-Gil, M.E. González-Molina, S. Mediavilla, A. Escudero, Estimation of chlorophyll in Quercus leaves using a portable chlorophyll meter: effects of species and leaf age, Ann. For. Sci. 67 (1) (2010) 108.
[74] C. Wu, Z. Niu, Q. Tang, W. Huang, Estimating chlorophyll content from hyperspectral vegetation indices: modeling and validation, Agric. For. Meteorol. 148 (8-9) (2008) 1230–1241.
[75] T.S. Hawkins, E.S. Gardiner, G.S. Comer, Modeling the relationship between extractable chlorophyll and SPAD-502 readings for endangered plant species research, J. Nat. Conserv. 17 (2) (2009) 123–127.